

# An Error Estimator for Electrically Coupled Liquid Crystals

J.H. Adler<sup>2</sup>[0000-0002-6603-8840] and D. B. Emerson<sup>1,2</sup>[0000-0002-4630-7003]

<sup>1</sup> Vector Institute, Toronto ON M5G 1M1, Canada  
david.emerson@vectorinstitute.ai

<sup>2</sup> Tufts University, Medford MA 02155, USA

**Abstract.** This paper extends an a posteriori error estimator for the elastic, Frank-Oseen model of liquid crystals, derived in [9], to include electric and flexoelectric effects. The problem involves a nonlinear coupled system of equations with a local unit-length constraint imposed via a penalty method. The proposed estimator is proven to be a reliable estimate of global approximation error. The performance of the coupled error estimator as a guide for adaptive refinement is shown in the numerical results, where the adapted grids successfully yield substantial reductions in computational work and comparable or better conformance to important physical laws.

**Keywords:** liquid crystals · a posteriori error estimators · adaptive mesh refinement.

## 1 Introduction

As materials possessing mesophases with characteristics of both liquids and organized solids, liquid crystals exhibit many interesting physical properties inspiring extensive study and a wide range of applications (eg. [10,17]). The focus of this paper is nematic liquid crystals, which are rod-like molecules with long-range orientational order described by a vector field  $\mathbf{n}(x, y, z) = (n_1, n_2, n_3)^T$ , known as the director, which is constrained to unit-length pointwise throughout the domain,  $\Omega$ . In addition to their elastic properties, liquid crystals are dielectrically active such that their structures are affected by the presence of electric fields. Certain liquid crystals also demonstrate flexoelectric coupling wherein deformations of the director produce internally generated electric fields [11].

With the combination of highly coupled physical phenomena and complicated experimental behavior, numerical simulations of liquid crystal structures are fundamental to the study of novel physical phenomena [13]. As such, the development of highly efficient and accurate numerical approaches is of significant importance. Effective a posteriori error estimators significantly increase the efficiency of numerical methods for partial differential equations and variational systems by guiding the construction of optimal discretizations via adaptive mesh refinement (AMR). A wealth of research exists for the design and theoretical support of effective error estimators in the context of finite-element methods [3,5].

In [9], a reliable a posteriori error estimator is developed for the first-order optimality conditions arising from minimization of the Frank-Oseen elastic free-energy model. Using the elastic estimator to guide AMR produced competitive solutions with considerably less computational work. In this work, the elastic error estimator is extended to consider systems with electric and flexoelectric coupling using a penalty approach to the required unit-length constraint. The proposed a posteriori error estimator is shown to be a reliable estimate of global approximation error. Numerical experiments with both external and flexoelectrically induced electric fields demonstrate the performance of the estimators compared with uniform refinement.

## 2 Free-Energy Model and Optimality Conditions

Liquid crystals are simulated using a number of different models [7,12]. We consider the Frank-Oseen free-energy model, where the coupled free-energy functional is

$$\begin{aligned} \mathcal{G}(\mathbf{n}, \phi) = & \frac{1}{2}K_1\|\nabla \cdot \mathbf{n}\|_0^2 + \frac{1}{2}K_3\langle \mathbf{Z}\nabla \times \mathbf{n}, \nabla \times \mathbf{n} \rangle_0 - \frac{1}{2}\epsilon_0\epsilon_{\perp}\langle \nabla\phi, \nabla\phi \rangle_0 \\ & - \frac{1}{2}\epsilon_0\epsilon_a\langle \mathbf{n} \cdot \nabla\phi, \mathbf{n} \cdot \nabla\phi \rangle_0 + e_s\langle \nabla \cdot \mathbf{n}, \mathbf{n} \cdot \nabla\phi \rangle_0 + e_b\langle \mathbf{n} \times \nabla \times \mathbf{n}, \nabla\phi \rangle_0. \end{aligned} \quad (2.1)$$

Here,  $K_i \geq 0$ ,  $i = 1, 2, 3$  are the Frank constants and, assuming that each  $K_i \neq 0$ ,  $\mathbf{Z} = \mathbf{I} - (1 - \kappa)\mathbf{n} \otimes \mathbf{n}$ , with  $\kappa = K_2/K_3$ . The variable  $\phi$  denotes the electric potential and  $\epsilon_0 > 0$  the permittivity of free space. The dielectric anisotropy of the liquid crystal is  $\epsilon_a = \epsilon_{\parallel} - \epsilon_{\perp}$ , with the constants  $\epsilon_{\parallel}, \epsilon_{\perp} > 0$  representing the parallel and perpendicular dielectric permittivity, respectively. Finally,  $e_s$  and  $e_b$  are material constants specifying the liquid crystal's flexoelectric response. Liquid crystal equilibrium states correspond to configurations that minimize the functional in (2.1) subject to the local unit-length constraint,  $\mathbf{n} \cdot \mathbf{n} - 1 = 0$ . Additionally, the relevant Maxwell's equations,  $\nabla \cdot \mathbf{D} = 0$  and  $\nabla \times \mathbf{E} = \mathbf{0}$ , must be satisfied. For this system,  $\mathbf{D} = -\epsilon_0\epsilon_{\perp}\nabla\phi - \epsilon_0\epsilon_a(\mathbf{n} \cdot \nabla\phi)\mathbf{n} + e_s\mathbf{n}(\nabla \cdot \mathbf{n}) + e_b(\mathbf{n} \times \nabla \times \mathbf{n})$ . Use of an electric potential implies that Faraday's law is trivially satisfied, and it is straightforward to show that a minimizing pair,  $(\mathbf{n}_*, \phi_*)$ , adhering to the unit-length constraint, satisfies Gauss' law in weak form. For a full derivation of the functional in (2.1), see [1,2].

Throughout this paper, we assume the presence of Dirichlet boundary conditions and that  $\mathbf{n} \in H_{\mathbf{g}_1}^1(\Omega)^3 = \{\mathbf{v} \in H^1(\Omega)^3 : \mathbf{v} = \mathbf{g}_1 \text{ on } \partial\Omega\}$  and  $\phi \in H_{g_2}^1(\Omega) = \{\psi \in H^1(\Omega) : \psi = g_2 \text{ on } \partial\Omega\}$ . The boundary functions  $\mathbf{g}_1$  and  $g_2$  satisfy appropriate compatibility conditions for the domain. Then, to obtain the variational form for the constrained optimization problem, we consider a penalty approach studied in [2]. The penalty method, for constant  $\zeta > 0$ , defines the energy as,  $\mathcal{H}(\mathbf{n}, \phi) = \mathcal{G}(\mathbf{n}, \phi) + \frac{1}{2}\zeta\langle \mathbf{n} \cdot \mathbf{n} - 1, \mathbf{n} \cdot \mathbf{n} - 1 \rangle_0$ . Taking the first variation of  $\mathcal{H}(\mathbf{n}, \phi)$ , the first-order optimality conditions are written,

$$\begin{aligned} \mathcal{P}(\mathbf{n}, \phi) = & K_1\langle \nabla \cdot \mathbf{n}, \nabla \cdot \mathbf{v} \rangle_0 + K_3\langle \mathbf{Z}\nabla \times \mathbf{n}, \nabla \times \mathbf{v} \rangle_0 + (K_2 - K_3)\langle \mathbf{n} \cdot \nabla \times \mathbf{n}, \mathbf{v} \cdot \nabla \times \mathbf{n} \rangle_0 \\ & - \epsilon_0\epsilon_a\langle \mathbf{n} \cdot \nabla\phi, \mathbf{v} \cdot \nabla\phi \rangle_0 - \epsilon_0\epsilon_{\perp}\langle \nabla\phi, \nabla\psi \rangle_0 - \epsilon_0\epsilon_a\langle \mathbf{n} \cdot \nabla\phi, \mathbf{n} \cdot \nabla\psi \rangle_0 \\ & + e_s(\langle \nabla \cdot \mathbf{n}, \mathbf{v} \cdot \nabla\phi \rangle_0 + \langle \nabla \cdot \mathbf{v}, \mathbf{n} \cdot \nabla\phi \rangle_0) + e_s\langle \nabla \cdot \mathbf{n}, \mathbf{n} \cdot \nabla\psi \rangle_0 \\ & + e_b(\langle \mathbf{n} \times \nabla \times \mathbf{n}, \nabla\phi \rangle_0 + \langle \mathbf{v} \times \nabla \times \mathbf{n}, \nabla\phi \rangle_0) + e_b\langle \mathbf{n} \times \nabla \times \mathbf{n}, \nabla\psi \rangle_0 \\ & + 2\zeta\langle \mathbf{v} \cdot \mathbf{n}, \mathbf{n} \cdot \mathbf{n} - 1 \rangle_0 = 0, \quad \forall(\mathbf{v}, \psi) \in H_0^1(\Omega)^3 \times H_0^1(\Omega). \end{aligned} \quad (2.2)$$

## 3 Reliable Coupled Error Estimators

In [9], a posteriori error estimators are proposed for elastic liquid crystal systems. In this section, the estimator for the penalty formulation is extended to include the electric and flexoelectric coupling described in Section 2. Furthermore, the estimator is shown to produce a reliable estimate of global approximation error.

### 3.1 Assumptions and Notation

Throughout, the domain  $\Omega$  is open and connected, with a polyhedral boundary. For any open subset  $\omega \subset \Omega$  with Lipschitz boundary, norms restricted to the subdomain are denoted with an index as

$\|\cdot\|_{1,\omega}$  and  $\|\cdot\|_{0,\omega}$ . Let  $\{\mathcal{T}_h\}$ ,  $0 < h \leq 1$ , be a quasi-uniform family of meshes subdividing  $\Omega$  with

$$\begin{aligned} \max\{\text{diam } T : T \in \mathcal{T}_h\} &\leq h \text{diam } \Omega, \\ \min\{\text{diam } B_T : T \in \mathcal{T}_h\} &\geq \rho h \text{diam } \Omega, \end{aligned} \quad (3.1)$$

where  $\rho > 0$  and  $B_T$  is the largest ball contained in  $T$  such that  $T$  is star-shaped with respect to  $B_T$ . In addition, we assume that any triangulation satisfies the admissibility condition such that any two cells of  $\mathcal{T}_h$  are either disjoint or share a complete, smooth sub-manifold of their boundaries. For any  $T \in \mathcal{T}_h$ , let  $h_T = \text{diam } T$ , denote the set of edges of  $T$  as  $\mathcal{E}(T)$ , and  $h_E = \text{diam } E$  for  $E \in \mathcal{E}(T)$ . It is also assumed that  $\mathcal{T}_h$  is fine enough that any  $h_T, h_E \leq 1$ . The quasi-uniformity condition of (3.1) ensures that the ratio  $h_T/h_E$  is bounded above and below by constants independent of  $h, T$ , and  $E$  and the smallest angle of any  $T$  is bounded from below by a constant independent of  $h$  [16].

The sets of vertices corresponding to  $T$  and  $E$  are written  $\mathcal{N}(T)$  and  $\mathcal{N}(E)$ , respectively. The set of all edges for  $\mathcal{T}_h$  is written  $\mathcal{E}_h = \bigcup_{T \in \mathcal{T}_h} \mathcal{E}(T)$ , and  $\mathcal{E}_{h,\Omega}$  signifies the subset of interior edges. Finally, some specific subdomains of  $\Omega$  are written

$$\begin{aligned} \omega_T &= \bigcup_{\mathcal{E}(T) \cap \mathcal{E}(T') \neq \emptyset} T', & \omega_E &= \bigcup_{E \in \mathcal{E}(T')} T', \\ \tilde{\omega}_T &= \bigcup_{\mathcal{N}(T) \cap \mathcal{N}(T') \neq \emptyset} T', & \tilde{\omega}_E &= \bigcup_{\mathcal{N}(E) \cap \mathcal{N}(T') \neq \emptyset} T'. \end{aligned}$$

The triangulation is assumed to be affine equivalent with reference elements  $\hat{T}$  and  $\hat{E}$ . For any edge,  $\eta_E$  is an outward facing normal on the boundary of  $E$ . For any piecewise continuous function  $\psi$ , the jump across  $E$  in the direction  $\eta_E$  is denoted as  $[\psi]_E$ .

For  $k \in \mathbb{N}$ , define the finite-dimensional space,  $S_h^{k,0} = \{\psi : \Omega \rightarrow \mathbb{R} : \psi|_T \in \Pi_k, \forall T \in \mathcal{T}_h\} \cap C(\bar{\Omega})$ , where  $\Pi_k$  is the set of polynomials of degree at most  $k$ , and  $\psi|_T$  is the restriction of  $\psi$  to the element  $T$ . Let  $I_h : L^1(\Omega) \rightarrow S_h^{1,0}$  denote the Clément interpolation operator [6]. Let  $\Psi_T$  and  $\Psi_E$  be cutoff functions and  $P : L^\infty(E) \rightarrow L^\infty(T)$  be a prolongation operator as defined in [15,16].

For Banach spaces  $X$  and  $Y$ , denote the space of continuous linear maps as  $\mathcal{L}(X, Y)$  with operator norm  $\|\cdot\|_{\mathcal{L}(X, Y)}$ . The subset of linear homeomorphisms is written  $\text{Isom}(X, Y)$ . Define  $Y^* = \mathcal{L}(Y, \mathbb{R})$  to be the dual space of  $Y$ , with norm  $\|\cdot\|_{Y^*}$ , where the associated duality pairing is written  $\langle \cdot, \cdot \rangle$ . Define  $C^1(X, Y^*)$  to be the set of continuously differentiable functions and a ball of radius  $R > 0$  centered at  $u \in X$  as  $B(u, R) = \{v \in X : \|u - v\|_X < R\}$ . Let  $X_h \subset X$  denote a finite-dimensional subspace. Finally, define the identity operator for a space  $Y$  as  $\text{Id}_Y$ , and let  $*$  indicate application of an action to the dual variables for a function from  $X \rightarrow Y^*$ . In the following, we make significant use of Proposition 2.1 and 2.5 from [16].

### 3.2 Penalty Error Estimator

To begin, consider the first-order optimality conditions in (2.2). Let  $Y = X_0 = H_0^1(\Omega)^3 \times H_0^1(\Omega)$  and  $X = H_{\mathbf{g}_1}^1(\Omega)^3 \times H_{g_2}^1(\Omega)$ . Then  $\mathcal{P}(\mathbf{n}, \phi) \in C^1(X, Y^*)$ , and the Dirichlet boundary conditions imply that for a fixed  $(\mathbf{n}, \phi) \in X$ ,  $D\mathcal{P}(\mathbf{n}, \phi) : X_0 \rightarrow Y^*$ , where  $D$  denotes the derivative. In discretizing the variational system, we consider general discrete spaces  $[S_h^{1,0}]^3 \subset V_h \subset [S_h^{s,0}]^3$ ,  $[S_h^{1,0}] \subset Q_h \subset [S_h^{t,0}]$ , for  $s, t \geq 1$ , and  $Y_h = \{(v_h, \psi_h) \in V_h \times Q_h : \mathbf{v}_h = \mathbf{0} \text{ and } \psi_h = 0 \text{ on } \Gamma\}$ . In the theory to follow, we assume that the boundary conditions for  $(\mathbf{n}, \phi)$  are exactly representable on the coarsest mesh of  $\{\mathcal{T}_h\}$ , which admits projection of the boundary functions  $\mathbf{g}_1$  and  $g_2$  onto the coarsest mesh. Hence,

$X_h = (V_h \times Q_h \cap X)$ . However, we note that, in the numerical results, any boundary condition functions are interpolated with mesh refinement.

For  $(\mathbf{v}, \psi) \in Y$  and  $\langle \mathcal{P}(\mathbf{n}, \phi), (\mathbf{v}, \psi) \rangle$  define the discrete approximation  $\langle \mathcal{P}_h(\mathbf{n}_h, \phi_h), (\mathbf{v}_h, \psi_h) \rangle := \langle \mathcal{P}(\mathbf{n}_h, \phi_h), (\mathbf{v}_h, \psi_h) \rangle$ , for  $(\mathbf{n}_h, \phi_h) \in X_h, (\mathbf{v}_h, \psi_h) \in Y_h$ . For the remainder of this section, assume that the pair  $(\mathbf{n}_h, \phi_h)$  is a solution to the discrete problem

$$\mathcal{P}_h(\mathbf{n}_h, \phi_h) = 0 \quad \forall (\mathbf{v}_h, \psi_h) \in Y_h. \quad (3.2)$$

In order to simplify notation, define the vector and scalar quantities

$$\begin{aligned} \mathbf{p} &= -K_1 \nabla(\nabla \cdot \mathbf{n}_h) + K_3 \nabla \times (\mathbf{Z}(\mathbf{n}_h) \nabla \times \mathbf{n}_h) + (K_2 - K_3)(\mathbf{n}_h \cdot \nabla \times \mathbf{n}_h) \nabla \times \mathbf{n}_h \\ &\quad + 2\zeta((\mathbf{n}_h \cdot \mathbf{n}_h - 1)\mathbf{n}_h) - \epsilon_0 \epsilon_a ((\mathbf{n}_h \cdot \nabla \phi_h) \nabla \phi_h) + e_s (\nabla \cdot \mathbf{n}_h) \nabla \phi_h \\ &\quad - e_s \nabla(\mathbf{n}_h \cdot \nabla \phi_h) + e_b (\nabla \times \mathbf{n}_h \times \nabla \phi_h) + e_b \nabla \times (\nabla \phi_h \times \mathbf{n}_h), \\ q &= \epsilon_0 \epsilon_\perp \Delta \phi_h + \epsilon_0 \epsilon_a \nabla \cdot ((\mathbf{n}_h \cdot \nabla \phi_h) \mathbf{n}_h) - e_s \nabla \cdot ((\nabla \cdot \mathbf{n}_h) \mathbf{n}_h) - e_b \nabla \cdot (\mathbf{n}_h \times \nabla \times \mathbf{n}_h), \\ \hat{\mathbf{p}} &= [K_1 (\nabla \cdot \mathbf{n}_h) \eta_E + K_3 (\mathbf{Z}(\mathbf{n}_h) \nabla \times \mathbf{n}_h) \times \eta_E + e_s (\mathbf{n}_h \cdot \nabla \phi_h) \eta_E + e_b ((\nabla \phi_h \times \mathbf{n}_h) \times \eta_E)]_E, \\ \hat{q} &= [-\epsilon_0 \epsilon_\perp (\nabla \phi_h \cdot \eta_E) - \epsilon_0 \epsilon_a (\mathbf{n}_h \cdot \nabla \phi_h) (\mathbf{n}_h \cdot \eta_E) + e_s ((\nabla \cdot \mathbf{n}_h) \mathbf{n}_h) \cdot \eta_E + e_b (\mathbf{n}_h \times \nabla \times \mathbf{n}_h) \cdot \eta_E]_E, \end{aligned}$$

where  $E \in \mathcal{E}_{h,\Omega}$ . Integrating  $\langle \mathcal{P}(\mathbf{n}_h, \phi_h), (\mathbf{v}, \psi) \rangle$  by parts elementwise for each  $T \in \mathcal{T}_h$ , using the fact that  $\mathbf{v}$  and  $\psi$  are zero on the boundary, and gathering terms yields

$$\langle \mathcal{P}(\mathbf{n}_h, \phi_h), (\mathbf{v}, \psi) \rangle = \sum_{T \in \mathcal{T}_h} \int_T \mathbf{p} \cdot \mathbf{v} dV + \int_T q \cdot \psi dV + \sum_{E \in \mathcal{E}_{h,\Omega}} \int_E \hat{\mathbf{p}} \cdot \mathbf{v} dS + \int_E \hat{q} \cdot \psi dS.$$

This form suggests a local estimator,

$$\Theta_T = \left\{ h_T^2 (\|\mathbf{p}\|_{0,T}^2 + \|q\|_{0,T}^2) + \sum_{E \in \mathcal{E}(T) \cap \mathcal{E}_{h,\Omega}} h_E (\|\hat{\mathbf{p}}\|_{0,E}^2 + \|\hat{q}\|_{0,E}^2) \right\}^{1/2},$$

for any  $T \in \mathcal{T}_h$ . Observe that the quantity  $\|q\|_{0,T}$  measures an approximation's local conformance to the strong form of Gauss' law.

### 3.3 Error Estimator Reliability

Using the assumptions of Section 3.1, a collection of intermediate lemmas, fundamental to the central reliability proof, are first established. Let  $R_h : Y \rightarrow Y_h$  be a restriction operator such that  $R_h(\mathbf{u}, \varphi) = (I_h u_1, I_h u_2, I_h u_3, I_h \varphi)$ . In order to remain consistent with the notation of [16, Proposition 2.5], we introduce the approximation  $\langle \tilde{\mathcal{P}}_h(\mathbf{n}_h, \phi_h), (\mathbf{v}, \psi) \rangle$ . However, as no forcing function or Neumann boundary conditions are present

$$\langle \tilde{\mathcal{P}}_h(\mathbf{n}_h, \phi_h), (\mathbf{v}, \psi) \rangle := \langle \mathcal{P}(\mathbf{n}_h, \phi_h), (\mathbf{v}, \psi) \rangle. \quad (3.3)$$

**Lemma 1.** *There exists a constant  $C > 0$  independent of  $h$  such that*

$$\|(Id_Y - R_h)^* \tilde{\mathcal{P}}_h(\mathbf{n}_h, \phi_h)\|_{Y^*} \leq C \left( \sum_{T \in \mathcal{T}_h} \Theta_T^2 \right)^{1/2}.$$

*Proof.* Applying the Cauchy-Schwarz inequality, standard error bounds of the Clément operator, and the Cauchy-Schwarz inequality for sums implies

$$\begin{aligned} & \|(\text{Id}_Y - R_h)^* \tilde{\mathcal{P}}_h(\mathbf{n}_h, \phi_h)\|_{Y^*} \\ & \leq \sup_{\substack{[\mathbf{v}, \psi] \in Y \\ \|[\mathbf{v}, \psi]\|_Y = 1}} \tilde{C} \left( \sum_{T \in \mathcal{T}_h} h_T^2 (\|\mathbf{p}\|_{0,T}^2 + \|q\|_{0,T}^2) + \sum_{E \in \mathcal{E}_{h,\Omega}} h_E (\|\hat{\mathbf{p}}\|_{0,E}^2 + \|\hat{q}\|_{0,E}^2) \right)^{1/2} \\ & \quad \cdot \left( \sum_{T \in \mathcal{T}_h} \|\mathbf{v}\|_{1,\tilde{\omega}_T}^2 + \|\psi\|_{1,\tilde{\omega}_T}^2 + \sum_{E \in \mathcal{E}_{h,\Omega}} \|\mathbf{v}\|_{1,\tilde{\omega}_E}^2 + \|\psi\|_{1,\tilde{\omega}_E}^2 \right)^{1/2}. \end{aligned}$$

There exists a constant  $C_* > 0$  independent of  $h$  taking into account repeated elements such that

$$\left( \sum_{T \in \mathcal{T}_h} \|\mathbf{v}\|_{1,\tilde{\omega}_T}^2 + \|\psi\|_{1,\tilde{\omega}_T}^2 + \sum_{E \in \mathcal{E}_{h,\Omega}} \|\mathbf{v}\|_{1,\tilde{\omega}_E}^2 + \|\psi\|_{1,\tilde{\omega}_E}^2 \right)^{1/2} \leq C_* \|[\mathbf{v}, \psi]\|_Y.$$

Noting that the jump components are summed over  $E \in \mathcal{E}_{h,\Omega}$  completes the proof.  $\square$

Next, define the finite-dimensional auxiliary space  $\tilde{Y}_h \subset Y$  as

$$\begin{aligned} \tilde{Y}_h = \text{span}\{ & [\Psi_T \mathbf{v}, 0], [\Psi_E P \sigma, 0], [\mathbf{0}, \Psi_T \psi], [\mathbf{0}, \Psi_E P \tau] \\ & : \mathbf{v} \in [\Pi_{k|_T}]^3, \sigma \in [\Pi_{k|_E}]^3, \psi \in \Pi_{l|_T}, \tau \in \Pi_{l|_E}, T \in \mathcal{T}_h, E \in \mathcal{E}_{h,\Omega}\}, \end{aligned}$$

where  $k \geq \max(3s, s + 2(t - 1))$  and  $l \geq 2s + (t - 1)$ . For this space, the following lemma holds.

**Lemma 2.** *There exists a  $C > 0$  independent of  $h$  such that  $\|\tilde{\mathcal{P}}_h(\mathbf{n}_h, \phi_h)\|_{\tilde{Y}_h^*} \leq C (\sum_{T \in \mathcal{T}_h} \Theta_T^2)^{1/2}$ .*

*Proof.* Applying the Cauchy-Schwarz inequality, using the definition of  $\tilde{Y}_h$ , quasi-uniformity of the mesh, and standard finite-element scaling arguments implies that

$$\begin{aligned} \|\tilde{\mathcal{P}}_h(\mathbf{n}_h, \phi_h)\|_{\tilde{Y}_h^*} & \leq \sup_{\substack{[\mathbf{v}_h, \psi_h] \in \tilde{Y}_h \\ \|[\mathbf{v}_h, \psi_h]\|_Y = 1}} \sum_{T \in \mathcal{T}_h} C_1 h_T \|\mathbf{p}\|_{0,T} \|\mathbf{v}_h\|_{1,T} + C_1 h_T \|q\|_{0,T} \|\psi_h\|_{1,T} \\ & \quad + \sum_{E \in \mathcal{E}_{h,\Omega}} C_2 h_E^{1/2} \|\hat{\mathbf{p}}\|_{0,E} \|\mathbf{v}_h\|_{1,\omega_E} + C_2 h_E^{1/2} \|\hat{q}\|_{0,E} \|\psi_h\|_{1,\omega_E}. \end{aligned}$$

Taking  $\tilde{C} = \max(C_1, C_2)$  and applying the Cauchy-Schwarz inequality for sums implies

$$\begin{aligned} \|\tilde{\mathcal{P}}_h(\mathbf{n}_h, \phi_h)\|_{\tilde{Y}_h^*} & \leq \sup_{\substack{[\mathbf{v}_h, \psi_h] \in \tilde{Y}_h \\ \|[\mathbf{v}_h, \psi_h]\|_Y = 1}} \tilde{C} \left( \sum_{T \in \mathcal{T}_h} h_T^2 (\|\mathbf{p}\|_{0,T}^2 + \|q\|_{0,T}^2) + \sum_{E \in \mathcal{E}_{h,\Omega}} h_E (\|\hat{\mathbf{p}}\|_{0,E}^2 + \|\hat{q}\|_{0,E}^2) \right)^{1/2} \\ & \quad \cdot \left( \sum_{T \in \mathcal{T}_h} \|\mathbf{v}_h\|_{1,T}^2 + \|\psi_h\|_{1,T}^2 + \sum_{E \in \mathcal{E}_{h,\Omega}} \|\mathbf{v}_h\|_{1,\omega_E}^2 + \|\psi_h\|_{1,\omega_E}^2 \right)^{1/2}. \end{aligned}$$

There exists a  $C_* > 0$ , independent of  $h$  and taking into account repeated elements, such that

$$\left( \sum_{T \in \mathcal{T}_h} \|\mathbf{v}_h\|_{1,T}^2 + \|\psi_h\|_{1,T}^2 + \sum_{E \in \mathcal{E}_{h,\Omega}} \|\mathbf{v}_h\|_{1,\omega_E}^2 + \|\psi_h\|_{1,\omega_E}^2 \right)^{1/2} \leq C_* \|[\mathbf{v}_h, \psi_h]\|_Y.$$

Again, noting that the jump components are summed over  $E \in \mathcal{E}_{h,\Omega}$  completes the proof.  $\square$

**Lemma 3.** *There exists a  $C > 0$  independent of  $h$  so that  $C (\sum_{T \in \mathcal{T}_h} \theta_T^2)^{1/2} \leq \|\tilde{\mathcal{P}}_h(\mathbf{n}_h, \phi_h)\|_{\tilde{Y}_h^*}$ .*

*Proof.* Fix an arbitrary  $T \in \mathcal{T}_h$  and edge  $E \in \mathcal{E}(T) \cap \mathcal{E}_{h,\Omega}$ . Further, define the restricted space  $\tilde{Y}_h|_\omega$ , for  $\omega \in \{T, \omega_E, \omega_T\}$ , as the set of functions  $\mathbf{f} \in \tilde{Y}_h$  with  $\text{supp}(\mathbf{f}) \subset \omega$ . Finally, denote the product spaces  $([\Pi_{k|T}]^3 \times \Pi_{l|T}) \setminus \{(\mathbf{0}, 0)\}$  and  $([\Pi_{k|E}]^3 \times \Pi_{l|E}) \setminus \{(\mathbf{0}, 0)\}$  as  $\Pi_{k,l,T}$ ,  $\Pi_{k,l,E}$ , respectively. Note that the constants in this proof correspond to those of [16, Lemma 3.3]. First, consider

$$C_1 C_4^{-1} h_T \|[\mathbf{p}, q]\|_{0,T} \leq \sup_{[\mathbf{w}, u] \in \Pi_{k,l,T}} C_4^{-1} h_T \|[\Psi_T \mathbf{w}, \Psi_T u]\|_{0,T}^{-1} \int_T (\mathbf{p}, q) \cdot (\Psi_T \mathbf{w}, \Psi_T u) dV \quad (3.4)$$

$$\leq \sup_{[\mathbf{w}, u] \in \Pi_{k,l,T}} \|[\Psi_T \mathbf{w}, \Psi_T u]\|_{1,T}^{-1} \int_T (\mathbf{p}, q) \cdot (\Psi_T \mathbf{w}, \Psi_T u) dV. \quad (3.5)$$

Inequalities (3.4) and (3.5) are given by applying Equations (3.1) and (3.3) from [16, Lemma 3.3], respectively. Noting that both  $\Psi_T \mathbf{w}$  and  $\Psi_T u$  vanish at the boundary of  $T$ ,

$$C_1 C_4^{-1} h_T \|[\mathbf{p}, q]\|_{0,T} \leq \sup_{\substack{[\mathbf{v}_h, \psi_h] \in \tilde{Y}_h|_T \\ \|[\mathbf{v}_h, \psi_h]\|_Y = 1}} \langle \tilde{\mathcal{P}}_h(\mathbf{n}_h, \phi_h), (\mathbf{v}_h, \psi_h) \rangle. \quad (3.6)$$

Next, by applying Equation (3.2) from [16, Lemma 3.3] and observing that the integrals and norms are taken over  $E$  where  $P$  does not modify the values of either  $\sigma$  or  $\beta$ ,

$$C_2 C_6^{-1} C_7^{-1} h_E^{1/2} \|[\hat{\mathbf{p}}, \hat{q}]\|_{0,E} \leq \sup_{[\sigma, \beta] \in \Pi_{k,l,E}} \frac{C_6^{-1} h_E}{C_7 h_E^{1/2} \| [P\sigma, P\beta] \|_{0,E}} \int_E (\hat{\mathbf{p}}, \hat{q}) \cdot (\Psi_E P\sigma, \Psi_E P\beta) dS.$$

Note that  $\Psi_E P\sigma$  is supported on  $\omega_E$ , and the norm in the denominator is taken over  $E$ . Applying Equation (3.5) of [16, Lemma 3.3] with  $C_7$  modified to consider each element of  $\omega_E$  implies

$$C_2 C_6^{-1} C_7^{-1} h_E^{1/2} \|[\hat{\mathbf{p}}, \hat{q}]\|_{0,E} \leq \sup_{[\sigma, \beta] \in \Pi_{k,l,E}} \frac{C_6^{-1} h_E}{\|[\Psi_E P\sigma, \Psi_E P\beta]\|_{0,\omega_E}} \left( \langle \tilde{\mathcal{P}}_h(\mathbf{n}_h, \phi_h), (\Psi_E P\sigma, \Psi_E P\beta) \rangle - \int_{\omega_E} (\mathbf{p}, q) \cdot (\Psi_E P\sigma, \Psi_E P\beta) dV \right),$$

Distributing the fraction and applying Equation (3.4) from [16, Lemma 3.3] to the first component and the Cauchy-Schwarz inequality to the second yields

$$\begin{aligned} & C_2 C_6^{-1} C_7^{-1} h_E^{1/2} \|[\hat{\mathbf{p}}, \hat{q}]\|_{0,E} \\ & \leq \sup_{[\sigma, \beta] \in \Pi_{k,l,E}} \|[\Psi_E P\sigma, \Psi_E P\beta]\|_{1,\omega_E}^{-1} \langle \tilde{\mathcal{P}}_h(\mathbf{n}_h, \phi_h), (\Psi_E P\sigma, \Psi_E P\beta) \rangle + C_6^{-1} h_E \sum_{T \in \omega_E} \|[\hat{\mathbf{p}}, \hat{q}]\|_{0,T} \\ & \leq \sup_{\substack{[\mathbf{v}_h, \psi_h] \in \tilde{Y}_h|_{\omega_E} \\ \|[\mathbf{v}_h, \psi_h]\|_Y = 1}} \|[\mathbf{v}_h, \psi_h]\|_{1,\omega_E}^{-1} \langle \tilde{\mathcal{P}}_h(\mathbf{n}_h, \phi_h), (\mathbf{v}_h, \psi_h) \rangle + C_d \sup_{\substack{[\mathbf{v}_h, \psi_h] \in \tilde{Y}_h|_{\omega_E} \\ \|[\mathbf{v}_h, \psi_h]\|_Y = 1}} \langle \tilde{\mathcal{P}}_h(\mathbf{n}_h, \phi_h), (\mathbf{v}_h, \psi_h) \rangle, \end{aligned}$$

where the final inequality is given by expanding the space over which the supremum is taken in the first summand and using Inequality (3.6), with  $C_d$  relating the constants  $C_6^{-1}h_E$  and  $C_1C_4^{-1}h_T$  and taking care of the summation over  $\omega_E$ . Note that the supremums only increase when taken over  $\omega_T$ . Gathering the bounds in (3.6) and the inequality above and using subadditivity of the square root for non-negative arguments implies

$$\bar{C}\Theta_T \leq \sup_{\substack{[\mathbf{v}_h, \psi_h] \in \tilde{Y}_h | \omega_T \\ \|[\mathbf{v}_h, \psi_h]\|_{Y^*} = 1}} \langle \tilde{\mathcal{P}}_h(\mathbf{n}_h, \phi_h), (\mathbf{v}_h, \psi_h) \rangle.$$

Finally, summing over  $T \in \mathcal{T}_h$  and again leveraging subadditivity completes the proof.  $\square$

The above results enable proof of the main theorem of this section.

**Theorem 1.** *Let  $(\mathbf{n}_*, \phi_*)$  be a solution to Equation (2.2) satisfying the assumptions of [16, Proposition 2.1]. Let  $(\mathbf{n}_h, \phi_h)$  be a discrete solution to Equation (3.2) such that  $\|\mathcal{P}_h(\mathbf{n}_h, \phi_h)\|_{Y^*} = 0$  and  $(\mathbf{n}_h, \phi_h) \in B((\mathbf{n}_*, \phi_*), R)$ . Then, there exist  $C_r > 0$ , independent of  $h$ , such that*

$$\|(\mathbf{n}_*, \phi_*) - (\mathbf{n}_h, \phi_h)\|_1 \leq C_r \left( \sum_{T \in \mathcal{T}_h} \Theta_T^2 \right)^{1/2}.$$

*Proof.* Combining Lemmas 1 and 3 implies the bound

$$\|(\text{Id}_Y - R_h)^* \tilde{\mathcal{P}}_h(\mathbf{n}_h, \phi_h)\|_{Y^*} \leq C_0 \left( \sum_{T \in \mathcal{T}_h} \Theta_T^2 \right)^{1/2} \leq C_1 \|\tilde{\mathcal{P}}_h(\mathbf{n}_h, \phi_h)\|_{\tilde{Y}_h^*}.$$

Thus, the conditions of [16, Proposition 2.5] are fulfilled. Noting from Definitions (3.2) and (3.3) that  $\|\mathcal{P}(\mathbf{n}_h, \phi_h) - \mathcal{P}_h(\mathbf{n}_h, \phi_h)\|_{Y^*} = 0$  and  $\|(\text{Id}_Y - R_h)^*[\mathcal{P}(\mathbf{n}_h, \phi_h) - \tilde{\mathcal{P}}_h(\mathbf{n}_h, \phi_h)]\|_{Y^*} = 0$ , and applying the result of Lemma 2,

$$\|\mathcal{P}(\mathbf{n}_h, \phi_h)\|_{Y^*} \leq C_2 \|\tilde{\mathcal{P}}_h(\mathbf{n}_h, \phi_h)\|_{\tilde{Y}_h^*} \leq C_3 \left( \sum_{T \in \mathcal{T}_h} \Theta_T^2 \right)^{1/2}.$$

It is straightforward to show that, for the defined Sobolev spaces and  $D\mathcal{P}(\mathbf{n}_*, \phi_*) \in \text{Isom}(X_0, Y)$ , [16, Proposition 2.1] still holds. The upper bound from that proposition implies that, for  $C_r = 2C_3\|D\mathcal{P}(\mathbf{n}_*, \phi_*)^{-1}\|_{\mathcal{L}(Y^*, X_0)}$ ,

$$\|(\mathbf{n}_*, \phi_*) - (\mathbf{n}_h, \phi_h)\|_1 \leq 2\|D\mathcal{P}(\mathbf{n}_*, \phi_*)^{-1}\|_{\mathcal{L}(Y^*, X_0)} \|\mathcal{P}(\mathbf{n}_h, \phi_h)\|_{Y^*} \leq C_r \left( \sum_{T \in \mathcal{T}_h} \Theta_T^2 \right)^{1/2}. \quad \square$$

## 4 Numerical Results

In this section, numerical experiments applying the electrically and flexoelectrically coupled estimator proposed above are presented. The numerical results suggest that the electrically coupled estimator markedly increases simulation efficiency with comparable or superior performance across a number of metrics compared with uniform mesh refinement.

The algorithm to compute solutions to the variational system discussed in Section 2 employs nested iteration (NI) [14]. The stopping criterion on each mesh is based on a tolerance of  $10^{-4}$  for the approximation's conformance to the first-order optimality conditions in the  $l_2$ -norm. For each iteration, an incomplete Newton correction is performed with damping parameter,  $\alpha$ , which begins at 0.2, increasing by 0.2 at each level of NI, to a maximum of 1.0. For additional details, see [1]. The system is discretized with  $Q_2$  (biquadratic) elements for both  $\mathbf{n}$  and  $\phi$ . On each level, AMR has three stages: Estimate  $\rightarrow$  Mark  $\rightarrow$  Refine. For each  $T \in \mathcal{T}_H$ , the local estimator  $\Theta_T$  is computed with respect to the coarse approximate solution  $\mathbf{u}_H$ . Elements of  $\mathcal{T}_H$  are then marked for refinement using Dorfler marking [8]. Any marked cells are refined through bisection to produce the next mesh. Grid management, discretizations, and adaptive refinement computations are implemented with the *deal.II* finite-element library [4]. All experiments are conducted on the same machine.

The simulations utilize meshes with quadrilateral elements. Therefore, adaptive refinement leads to the existence of hanging nodes. These nodes are dealt with in a standard way to maintain continuity along the boundary. Additionally, a 1-irregular mesh is maintained such that the number of hanging nodes on an edge is at most one. It should be noted that the theory developed in preceding sections assumes that the studied meshes satisfy the admissibility property. In the numerical experiments, this assumption is valid for the coarsest mesh but, with the introduction of hanging nodes, no longer strictly holds after the first AMR stage. Thus, after the first level of refinement, the error estimator is applied heuristically.

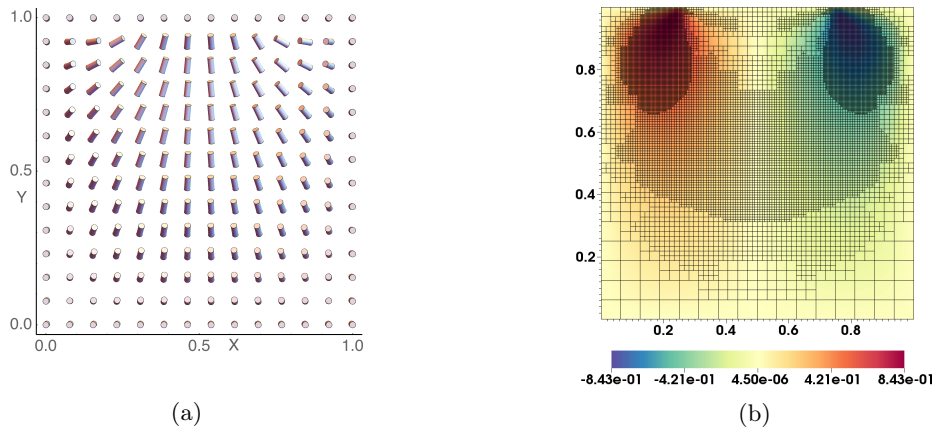


Fig. 1: (a) Fine-mesh computed solution (restricted for visualization). (b) Resulting mesh patterns after four levels of AMR overlaid on the value of  $n_1$ .

In order to quantify efficiency, an approximate work unit (WU) is calculated for each simulation. A WU roughly approximates the work required by any full NI hierarchy in terms of assembling and solving a single linearization step for the Hessian on the finest uniform mesh when optimally scaling solvers are applied. For a full definition, see [9]. While the linear systems here are solved with simple LU decomposition, the reported WUs provide a best-case scaling for comparing the work required between AMR and uniform refinement.

The experiments below consider a liquid crystal system with a large applied electric field and flexoelectric coupling on a unit-square domain. The non-dimensionalized physical parameters for 5CB, a common liquid crystal, are used such that  $K_1 = 1$ ,  $K_2 = 0.62903$ ,  $K_3 = 1.32258$ ,  $\epsilon_{\perp} = 7$ , and  $\epsilon_a = 11.5$ . The non-dimensionalized free-space permittivity is  $\epsilon_0 = 1.42809$ , and the flexoelectric



constants are  $e_s = 1.5$  and  $e_b = -1.5$ . Finally, the penalty parameter is  $\zeta = 10^5$ . Each of the simulations begins on a  $16 \times 16$  mesh followed by 5 levels of uniform refinement or 6 levels of AMR. At all boundaries  $\mathbf{n} = (0, 0, 1)^T$ . The electric potential is set to zero except along  $y = 1.0$  where an approximate square function is used such that  $\phi$  rises to 1.5 on roughly the middle-third of the edge, producing a large electric field with a sharp transition near the top boundary.

The effects of the electric field are seen in Figure 1a, which shows the computed solution on the finest mesh resulting from Dorfler AMR with parameter  $\nu = 0.9$ . In response to the field, the director deforms to align with the field lines, even near the boundary where elastic resistance is strongest. The regions surrounding the rapid transitions in the electric potential contain the most difficult to resolve physics and the largest free energy contributions, which suggests that a significant portion of the total approximation error will also be present in these areas. In Figure 1b, the refinement pattern resulting from AMR clearly emphasize these transition regions.

Table 1: Statistics associated with solutions computed with AMR vs. uniform refinement.

Refinement	Max $ \mathbf{n} \cdot \mathbf{n} - 1 $	Gauss Law	Free Energy	DOFs	WUs	Timing
Uniform	4.472e-02	357.844	-39.4858	4.202e06	4.764	7, 174s
AMR	4.460e-02	101.794	-39.4726	2.640e06	2.427	2, 700s

While no known analytical solution exists for this problem, there are a number of indicative metrics that facilitate comparison of computed numerical solutions. Table 1 presents these statistics contrasting the quality of approximate solutions produced on uniform meshes with those computed through AMR. As expected, computing a solution using AMR takes considerably less time and consumes half the WUs. The AMR solution exhibits slightly tighter unit-length conformance, measured by the solutions maximum unit length deviation at the quadrature nodes, and commensurate free energy compared to the solution on the finest uniform mesh. Finally, the table reports each solution’s local Gauss’ law conformance over the domain, measured as  $\sum_{T \in \mathcal{T}_h} \int_T (\nabla \cdot \mathbf{D})^2 dV$ . As no special consideration or care has been taken to strongly enforce conformance, outside of adherence to the first-order optimality conditions, the sharp boundary conditions of the electric potential lead to relatively large values. However, the AMR solution’s conformance is markedly better, implying more accurate capture of the relevant physics.

## 5 Conclusion and Future Work

We have discussed an a posteriori error estimator for the electrically and flexoelectrically coupled Frank-Oseen models of nematic liquid crystals, which provide a reliable estimate of global approximation error. The numerical results suggest that the estimator is highly effective in guiding AMR, producing measurably better solutions with less computational work. Future work will include extending the theoretical framework to demonstrate reliability and efficiency of the error estimator associated with the Lagrange multiplier formulation.

**Acknowledgments** The authors would like to thank Professor Xiaozhe Hu for his helpful suggestions along with Dr. Melody Takeuchi and Divya Sivasankaran for their careful readings.

## References

1. Adler, J.H., Atherton, T.J., Benson, T.R., Emerson, D.B., MacLachlan, S.P.: Energy minimization for liquid crystal equilibrium with electric and flexoelectric effects. *SIAM J. Sci. Comput.* **37**(5), S157–S176 (2015)

2. Adler, J.H., Emerson, D.B., MacLachlan, S.P., Manteuffel, T.A.: Constrained optimization for liquid crystal equilibria. *SIAM J. Sci. Comput.* **38**(1), B50–B76 (2016)
3. Babuska, I., Rheinboldt, W.C.: A posteriori error estimates for the finite element method. *Int. J. Numer. Meth. Engng* (12), 1597–1615 (1978)
4. Bangerth, W., Hartmann, R., Kanschat, G.: deal.II – a general purpose object oriented finite element library. *ACM Trans. Math. Softw.* **33**(4), 24/1–24/27 (2007)
5. Bank, R.E., Welfert, D.B.: A posteriori error estimators for elliptic partial differential equations. *Math. Comp.* **44**, 283–301 (1985)
6. Clément, P.: Approximation by finite element functions using local regularization. *RAIRO Anal. Numér.* **2**, 77–84 (1975)
7. Davis, T.A., Gartland-Jr., E.C.: Finite element analysis of the Landau-de Gennes minimization problem for liquid crystals. *SIAM J. Numer. Anal.* **35**(1), 336–362 (1998)
8. Döfler, W.: A convergent adaptive algorithm for Poisson’s equation. *SIAM J. Numer. Anal.* **33**, 1106–1124 (1996)
9. Emerson, D.B.: A posteriori error estimates for the Frank-Oseen model of liquid crystals. *J. Coupled Syst. Multiscale Dyn.* **5**(2), 95–110 (2017)
10. Lagerwall, J.P.F., Scalia, G.: A new era for liquid crystal research: Applications of liquid crystals in soft matter, nano-, bio- and microtechnology. *Curr. Appl. Phys.* **12**(6), 1387–1412 (2012)
11. Meyer, R.B.: Piezoelectric effects in liquid crystals. *Phys. Rev. Lett.* **22**(18), 918–921 (1969)
12. Onsager, L.: The effects of shape on the interaction of colloidal particles. *Ann. NY Acad. Sci.* **51**, 627–659 (1949)
13. Rojas-Gómez, O.A., Romero-Enrique, J.M., Silvestre, N.M., da Gama, M.M.T.: Pattern-induced anchoring transitions in nematic liquid crystals. *J. Phys. Condens. Matter* **29**(6) (2017)
14. Starke, G.: Gauss-Newton multilevel methods for least-squares finite element computations of variably saturated subsurface flow. *Computing* **64**, 323–338 (2000)
15. Verfürth, R.: A posteriori error estimates for nonlinear problems. Finite element discretizations of elliptic equations. *Math. Comp.* **62**(206), 445–475 (1994)
16. Verfürth, R.: A Review of A Posteriori Error Estimation and Adaptive Mesh-Refinement Techniques. Wiley and Teubner (1996)
17. Wan, Y., Zhao, D.: On the controllable soft-templating approach to mesoporous silicates. *Chem. Rev.* **107**(7), 2821–2860 (2007)